Modeling surface topography of state-of-the-art x-ray mirrors as a result of stochastic polishing process: recent developments

Valeriy V. Yashchuk,*[a] Gary Centers,[a] Yury N. Tyurin,[b,c] and Anastasia Tyurina,[c]
[a]Advanced Light Source, Lawrence Berkeley National Laboratory, One Cyclotron Rd., Berkeley, CA, USA 94720; [b]Moscow State University, 1 Leninskiye Gory St., Moscow, Russia 119991; [c]Second Star Algonumerix, 19 West St., Needham, Massachusetts, USA 02494

ABSTRACT

Recently, an original method for the statistical modeling of surface topography of state-of-the-art mirrors for usage in x-ray optical systems at light source facilities and for astronomical telescopes [Opt. Eng. 51(4), 046501, 2012; ibid. 53(8), 084102 (2014); and ibid. 55(7), 074106 (2016)] has been developed. In modeling, the mirror surface topography is considered to be a result of a stationary uniform stochastic polishing process and the best fit time-invariant linear filter (TILF) that optimally parameterizes, with limited number of parameters, the polishing process is determined. The TILF model allows the surface slope profile of an optic with a newly desired specification to be reliably forecast before fabrication. With the forecast data, representative numerical evaluations of expected performance of the prospective mirrors in optical systems under development become possible [Opt. Eng., 54(2), 025108 (2015)]. Here, we suggest and demonstrate an analytical approach for accounting the imperfections of the used metrology instruments, which are described by the instrumental point spread function, in the TILF modeling. The efficacy of the approach is demonstrated with numerical simulations for correction of measurements performed with an autocollimator based surface slope profiler. Besides solving this major metrological problem, the results of the present work open an avenue for developing analytical and computational tools for stitching data in the statistical domain, obtained using multiple metrology instruments measuring significantly different bandwidths of spatial wavelengths.

Keywords: Surface metrology, time-invariant linear filter, parametrization, point spread function, modulation transfer function, power spectral density, metrology of x-ray optics, calibration

1. INTRODUCTION

Recently, an original method for the statistical modeling of the stochastic part of surface topography of state-of-the-art mirrors for usage in x-ray optical systems at light source facilities and for astronomical telescopes has been developed.[1-6] In modeling, the mirror surface topography, after subtraction of the mirror non-stochastic shape (trend), is considered to be the result of a stationary uniform stochastic polishing process; and a best fit time-invariant linear filter (TILF) that optimally parameterizes, with limited number of parameters, the polishing process results is determined. The dedicated software is under development in the scope of NASA STTR/SBIR program.

The TILF model, when determined, allows the surface slope profile of an optic with a newly desired specification to be reliably forecast before fabrication. With the forecast data, representative numerical evaluations of expected performance of the prospective mirrors in optical systems under development become possible.[7,8] Moreover, the modeling could potentially provide a feedback to the deterministic polishing processes, avoiding time-consuming whole scale metrology measurements over the entire optical surface at the resolution required to cover the desired spatial frequency range. The work in this direction is also in progress.

Here, we initiate a new project devoted to one more possible application of the developed methods of statistical modeling. This is a development of a single-model (hybrid) statistical description of stochastic topography data for a surface under test (SUT) obtained through a number of metrology instruments designed for measurements over significantly different ranges of spatial wavelength. This can be thought of as data stitching in statistical domain, or 'statistical stitching.'

The importance of this project can be justified by the following discussion.

*VVYashchuk@lbl.gov; phone 1 510 495-2592; fax 1 510 486-7696

Generally, depending on the application of a mirror in a particular optical system, the spatial wavelength range of interest varies from a few nanometers (reachable, for example, with electron, x-ray, and/or atomic force microscopes) up to the whole size of a SUT with a length of ~ 1 meter (accessible, for example, with optical interferometers and slope measuring profilers). There is no metrology tool capable of covering the entire spatial wavelength range in a single measurement.

A limited increase of spatial wavelength range characterized from the data is possible with stitching of multiple identical (performed with the same metrology tool) measurements made with translation of the tool across the SUT.[9,10] Such stitching leads to a proportional increase of the data volume, measuring time, and the required set-up stability. Moreover, such straightforward stitching does not solve the problem of combining dissimilar data from principally different instruments.

As mentioned above, the core of the project started here is development of analytical methods for stitching dissimilar metrology data in the statistical domain. The project is based on the developed methods of statistical modeling of the metrology data treated as a result of a stochastic process.[1-6] In this case, the data from each instrument is modeled independently. The resulted models, each applicable to the spatial wavelength range determined by the particular instrument, are combined to a single hybrid model that reproduces the statistical properties of the SUT over the spatial wavelength range covered by all the instruments in use.

One of the major problems to be solved in the scope of the project is reliable accounting of the imperfections in the instruments used to obtain the surface topography data. The effects of imperfection in measuring instruments, expressed in terms of the point spread function (PSF) and modulation transfer function (MTF),[11] to the authenticity and mutual consistency of power spectral density (PSD) distributions obtained from a series of measurements of the same surface under test using different metrology instruments have been comprehensively discussed in literature [see, for example, Refs.[12-17] and reference therein].

In this paper, we suggest and demonstrate an analytical approach to reliably account for the imperfections of the used metrology instruments, which are described by the instrumental PSF, in the TILF modeling. The paper is organized as follows: In Sec. 2 we briefly review the modern methods of characterization of metrology instrumentation, concentrating on MTF correction of metrology data in the spatial frequency domain, and provide the corresponding relations between the MTF, PSF and the instrumental optical transfer function (OTF). A brief review of mathematical foundations of the stochastic modeling of surface metrology data is given in Sec. 3. The PSF correction in the statistics domain is discussed in Sec. 4 for the case of a reversible PSF. In Sec. 5, we derive analytical expressions for the OTF and PSF of an autocollimator based surface slope profiler. However, the corresponding PSF is irreversible so an analytical recipe for overcoming the irreversibility problem is considered in Sec. 6. It is based on application of approximate correction methods developed for restoration of blurred images. In Sec. 7, the efficacy of the correction is demonstrated with numerical simulations of correction for measurements performed with an autocollimator based surface slope profiler. The paper concludes (Sec. 8) by summarizing the main concepts discussed through the paper and outlining a plan for future work.

2. INSTRUMENTAL PERTRUBATION OF METROLOGY DATA

As an illustration of the problem related to the instrumental MTF, we refer to the publications,[12-15] where one-dimensional (1D) power spectral density (PSD) spectra obtained from an Au-coated Ni-plated and Au-coated polished stainless-steel (SS) x-ray mirrors are presented as measured with an atomic force microscope (AFM) Dimension-3100, an optical interferometric microscope MicroMapTM-570, a 6-in Fizeau interferometer ZYGO GPI, and a slope measuring long trace profiler (LTP). All the instruments are available at the Advanced Light Source (ALS) X-Ray Optics Laboratory (XROL).[18,19]

The comparison of the PSD spectra depicts strong discrepancy of the data from different instruments, as well as the ones from the same instrument, the interferometric microscope, equipped with different objectives, providing different sizes of field-of-view and the spatial resolution. The discrepancy is due to the limited resolution of the instruments that is seen as the PSD's strong roll-off at the higher spatial frequencies accessible with a particular instrument.

The roll-off like perturbation of the PSD spectra is a signature of the instrumental MTF. If the MTFs of the metrology instruments in use are known (for example, via specially arranged MTF calibration tests; see, for example, Refs.[20-29] and

references therein), the PSDs measured with a SUT can be corrected providing significantly more reliable information about the inherent PSD of the SUT over the entire spatial wavelength range, covered by the instruments.

Below, we briefly review the methods for the MTF calibration of different surface profilers.

2.1 MTF calibration and correction of metrology data in spatial frequency domain

To the extent that the response of the instrument can be characterized as a linear and shift-invariant system, the measured PSD is a product of the PSD inherent for the sample, PSD_{sample}, and the MTFs of the individual components (objective, detector, etc.) of the instrument:

$$PSD_{measured} = PSD_{sample} \times MTF^2 . \quad (1)$$

In Eq. (1), MTF is the total MTF of the instrument. It can be experimentally determined by comparing the measured PSD distribution of a test surface to the corresponding ideal PSD distribution, which is numerically simulated or found from PSD measurements with an instrument of significantly higher resolution.

There are a number of well-established methods for MTF calibration of different surface profilers. For example, a very efficient and universal experimental method for the MTF calibration of a broad range of surface profilometers, including large field-of-view Fizeau interferometers, optical interferometric microscopes, and scanning and transmission electron and x-ray microscopes has been recently developed and demonstrated.[20-29] The method is based on binary pseudo-random (BPR) one-dimensional sequences and two-dimensional (2D) arrays.[30-36] The universality of the approach based on BPR test samples, making it suitable for MTF characterization of fundamentally different instruments, is ensured by the similarity of specification of the test samples as sets (1D sequences, or 2D arrays) of pseudo-randomly distributed elements with a binary (two-level) physical property such as two height levels or two materials with different physical properties (for example: x-ray and electron beam transmission, reflectivity, electrical conductivity, magnetic permeability, etc).

For the MTF calibration of slope measuring profilers, a method based on specially designed chirped profiles has been recently developed and demonstrated.[37,38] In Sec. 4, we consider the MTF of an autocollimator based surface slope profiler in more detail and provide its analytical description.

2.2 Relation between the instrumental PSF, OTF, and MTF

If a metrology instrument is linear and shift invariant, the instrumental aberrations can be characterized by its point spread function. The PSF describes its response to a point (delta-function-like) topographic object (see, for example, Refs.[11,16,17]). The effect of the PSF to the surface measurements can be thought of as application of the corresponding filter PSF to the topography under test. Therefore, in the 1D case, a measured trace X_{MES} can be presented as:

$$X_{MES} = PSF * X_{SUT} + N_{MES} , \quad (2)$$

where X_{SUT} is the trace, corresponding to the inherent (unperturbed by the measurement) SUT topography. In Eq. 2, the symbol '*' denotes the convolution operation. The additive noise N_{MES} is due to random errors of the measurement, such as, for example, the CCD detector dark current noise. N_{MES} is assumed to be described with zero-mean variance white Gaussian noise (referred to as 'white Gaussian noise'), and, therefore, uncorrelated with X_{SUT}.

The optical transfer function (OTF), defined as the Fourier transform of the PSF,[11]

$$OTF = Fourier[PSF] \equiv F[PSF] , \quad (3)$$

is closely related to the instrumental MTF:

$$OTF \equiv MTF \exp(-i\, PTF) . \quad (4)$$

The OTF when it squared is equal to MTF^2 in Eq. (1). The difference between the OTF and MTF is in the phase transfer function, PTF; see Eq. (4). For a symmetrical PSF centered on the ideal image point (this is usually the case of surface topology measurements with state-of-the-art metrology instruments), the PTF as a function of spatial frequency

has only a value of either zero or π. Correspondingly, the OTF is a real bipolar function (with regions of positive and negative values), whereas the MTF is only positively defined.[11]

From the consideration above, it follows that a straightforward reconstruction of the PSF from the MTF measurements is generally impossible. Nevertheless, the problem can be solved if the instrumental PSF can be analytically modeled. Then, the measured MTF can be used to find parameters of the corresponding PSF model.[29] In Sec. 5, we will show that for the case of the slope profiler, direct analytical derivation of the instrumental OTF is also possible.

For the purpose of the present work, the important conclusion is that it is generally possible to reconstruct or, at least, to get a good guess for the MTF and PSF from experimental calibration of the instrument. If this is the case, the knowledge of the experimental PSF can be used to account the instrumental perturbation in the measured surface topography and, correspondingly, in the stochastic model describing the topography. This can result in significantly increased reliability of the measurements, enable stitching of different instrumental data in the statistical domain, and increase the effective resolution of the instrument.

3. MATHEMATICAL FOUNDATIONS OF THE STOCHASTIC MODELING OF MIRROR SURFACE SLOPE TOPOGRAPHY

3.1 1D ARMA modeling

Let us consider the result of measurement of 1D surface slope topography of a high quality x-ray mirror that is a distribution (trace) of residual (after subtraction of the best fit figure and trends) slopes $X[n]$ measured over discrete points $x_n = n \cdot \Delta x$ [$n = 1,...,N$, where N is the total number of observations, and $(N-1)\Delta x$ is the total length of the trace], uniformly, with an increment Δx, distributed along the trace.

ARMA modeling describes the discrete surface slope distribution $X[n]$ as a result of a uniform stochastic process (that is the polishing process):[1,2,16,17]

$$X[n] = \sum_{l=1}^{p} a_l X[n-l] + \sum_{l=0}^{q} b_l \nu[n-l], \tag{5}$$

where $\nu[n]$ is zero-mean unit-variance white Gaussian noise (referred to as 'white Gaussian noise') that is the driving noise of the model. The parameters p and q are the orders of the autoregressive and moving average processes, respectively. At $q = 0$ and $b_0 = 1$, the ARMA process (1) reduces to an AR stochastic process. Additional to the linearity, the ARMA transformation is time-invariant since its coefficients depend on the relative lags, l, rather than on n. The goal of the modeling is to determine the ARMA orders and estimate the corresponding AR and MA coefficients a_l and b_l. In the 1D case, the ARMA model parameters can be determined with commercially available software, such as EViews.[39] The software also allows to verify the statistical reliability of the model.

Trustworthy ARMA modeling and forecasting based on a limited number of observations assumes statistical stability of the data used. The data are statistically stable if they are the result of a so called wide sense stationary (WSS) random process (see, for example, Ref.[16]). The process $X[n]$ is a WSS process if its auto-covariance function (ACF),

$$r_X[l] = E(X[n]X[n-l]), \tag{6}$$

depends only on the lag l, and does not depend on the value of n. In (6) E is the expectation operator.

When an ARMA model is identified, the corresponding PSD distribution can be analytically derived:[16]

$$P_X(f) = \sigma^2 \frac{(b_0 + b_1 z^{-1} + \ldots + b_q z^{-q})(b_0 + b_1 z^{1} + \ldots + b_q z^{q})}{(1 - a_1 z^{-1} - \ldots - a_p z^{-p})(1 - a_1 z^{1} - \ldots - a_p z^{p})}, \tag{7}$$

where the frequency $f \in [-0.5, 0.5]$, $z = e^{i2\pi f}$, and σ^2 is the variance of the driving noise $\nu[n]$.

Therefore, a low-order ARMA fit, if successful, allows parametrization of the PSD (and the ACF) of a random rough surface. As a result, the analytical PSD distributions (6) appear as highly smoothed versions of the corresponding

estimates via a direct digital Fourier transform providing a possibility for model-based extrapolation of the PSD spectra outside the measured bandwidth.[1,2]

Examples of successful application of ARMA modeling to the experimental surface slope data for high quality x-ray mirrors can be found in Refs.[1-8]

With the obvious success and perspective of the application of 1D ARMA modeling to 1D residual surface slope topography of x-ray mirrors, the ARMA modeling is inherently causal, assuming that the current value of the process depends only upon the past points. This can be thought as a limiting factor because it generally contradicts the nature of optical polishing, and additionally, it complicates extension of the method for modeling two-dimensional (2D) surface topography available, for example, with optical interferometers and microscopes.

The causality limitation can be easily solved by a straightforward merging of the causal ARMA processes determined for the direct and reversed residual slope traces into a 'two-sided' ARMA model:[3,4]

$$X[n] = \frac{1}{2}\left\{\sum_{l=1}^{p}\left(a_l^* X[n+l] + a_l X[n-l]\right) + \sum_{l=0}^{q}\left(b_l^* \nu[n+l] + b_l \nu[n-l]\right)\right\}, \tag{8}$$

where the terms with the weights marked with the star symbol corresponds to the causal ARMA model of the reversed trace.

3.2 1D TILF modeling

For the 1D case, the time-invariant linear filter C with weights $\{c_i, i = 0, \pm 1, ...\}$ is a linear operator that transforms one stochastic process $\{X[t], t = 0, \pm 1, ...\}$ into another (filtered) process $\{Y[t], t = 0, \pm 1, ...\}$:[3-6,40]

$$Y[t] = \sum_{l=-\infty}^{\infty} c_l X[t-l] \equiv C * X[t]. \tag{9}$$

Similar to the ARMA transformation, the TILF C is linear and time-invariant. The requirement of stability of the transformation implies that the filter is absolutely summable:

$$\sum_{l=-\infty}^{\infty} |c_l| < \infty. \tag{10}$$

Similar to ARMA modeling, when an optimal TILF is identified, the corresponding power spectral density distribution can be analytically derived:

$$P_Y(f) = \left|\sum_{l=-\infty}^{\infty} c_l\, e^{i2\pi l f}\right|^2 P_X(f). \tag{11}$$

Almost any ARMA process $X[t]$ with the parameters p and q can be obtained from white Gaussian noise $\nu[t]$ by application of the corresponding casual TILF:[40]

$$X[t] = \sum_{l=0}^{\infty} c_l\, \nu[t-l] \tag{12}$$

with the weights c_l given by:

$$\sum_{l=0}^{\infty} c_l\, z^l = b(z)/a(z), \quad |z| \le 1, \tag{13}$$

where the AR and MA polynomials in the right hand side of Eq. (13) are, respectively [compare with Eq. (7)],

$$a(z) = 1 - a_1 z^1 - \ldots - a_p z^p \quad \text{and} \quad b(z) = 1 + b_1 z^1 + \ldots + b_q z^q. \tag{14}$$

The free of the causality limitation 'two-sided ARMA' process (8) can also be expressed via a TILF:

$$X[t]=\frac{1}{2}\left\{\sum_{l=0}^{\infty}c_l\,\nu[t-l]+\sum_{l=0}^{\infty}c_{-l}\,\nu[t+l]\right\}=\sum_{l=-\infty}^{\infty}c_l^{*}\,\nu[t-l]\,. \tag{15}$$

Therefore in the case of 1D surface topography data, if ARMA modeling is successful, there is a corresponding TILF operator that describes the topography as a result of filtering white Gaussian noise. The identified TILF can be used for forecasting a new slope distribution possessing the same statistical properties as the measured one, but with different parameters, such as the distribution length and the root-mean-square (rms) variation.

Below in Sec. 4, we use a TILF that transforms the 'two-sided AR' process into a white Gaussian noise process:[3,4]

$$\nu[t]=\sum_{l=-p}^{p}c_l\,X[t-l]-X[t]\equiv(C-I)*X[t]\,, \tag{16}$$

where I is the identity operator, and C a finite time-invariant linear filter of order p with the weights

$$c_l=a_l/2\,,\ \text{for}\ \ l=\pm1,...,\pm p\,,\ \text{and}\ c_0=0\,,\ \text{for}\ \ l=0\,. \tag{17}$$

In some sense the TILF $(C-I)$ in Eq. (16) is the inverse operator to the one given by Eq. (15).

Filter C in expression (16), when applied to the process $X[t]$, gives a new stationary random process $Y[t]$ that differs from the process $X[t]$ by the noise process $\nu[t]$ [compare with definition (9)]. If the difference is small (e.g., the variance of the noise is much smaller of that of the processes $X[t]$ and $Y[t]$), the TILF C can be thought as a good model of the stochastic process $X[t]$, representing its structure with the weight coefficients given by Eq. (17).

Practically, in order to determine a TILF filter C that best models the observed stochastic process $X[t]$, one has to find a set of the weight coefficients c_l that minimizes the deviation

$$E\left(\left[X[t]-Y[t]\right]^2\right)\equiv E\left(\nu^2[t]\right) \tag{18}$$

of the modeled process from the observed one.

3.3 Optimal symmetrical TILF

Generally, the values of the TILF weights with the same positive and negative lags are not necessarily equal, that is

$$c_l\neq c_{-l}\,. \tag{19}$$

However, as mathematically proved in Refs.,[5,6] among all TILFs (including AR and ARMA models) of the same order, the symmetrical filter with

$$c_l=c_{-l} \tag{20}$$

provides the smallest variance of the residual noise $E\left(\nu^2[t]\right)$. In the case of TILFs in the form of two-sided AR and ARMA models, it can be intuitively understood as a result of averaging of the residual noises of the fits with the corresponding causal filters of the direct and reversed processes. Assuming that the residual noises are not mutually correlated, one should expect a suppression of the variance of the averaged residual noise by a factor of two with respect to the corresponding causal filter.

The key task is the identification of an optimal TILF that best models (with minimum number of parameters and with the smallest possible residual noise) the observed stationary stochastic process. An original algorithm for direct optimization of the TILF model without involving results of the ARMA modeling has been derived in Refs.[5,6]

A condition for determining the weight coefficients of the optimal symmetric TILF C of the order p defined with weight coefficients $c_1,\ldots,c_p$ is:[5,6]

$$\vec{c}=\vec{r}_X Q^{-1}\,, \tag{21}$$

where Q is a $p \times p$ matrix with the elements $q[k,l]$ built of the coefficients for the auto-covariance function of the process $X[t]$:

$$q[k,l] \equiv r_X[k+l] + r_X[k-l] = r_X[|k+l|] + r_X[|k-l|]; \quad 1 \le k, l \le p, \tag{22}$$

and the vectors $\vec{c}$ of the TILF weights and $\vec{r}_X$ of the process auto-covariance are $\vec{c} \equiv \langle c_1, \ldots, c_p \rangle$ and $\vec{r}_X \equiv \langle r_X[1], \ldots, r_X[p] \rangle$. Note that expression (21) assumes existence of the inverse of matrix Q.

The expression for calculating the minimum value of the variance between the observed process $X[t]$ and the approximating one, $Y[t]$, is

$$E\left(\left[X[t] - Y[t] \right]^2 \right)_{MIN} = r_X[0] - 2\vec{r}_X \, Q^{-1} \, \vec{r}_X{}^T . \tag{23}$$

Equations (22) and (23) provide an algorithm for evaluation of the best TILF with given order p.

4. THE PSF CORRECTION IN THE STATISTICS DOMAIN: THE CASE OF A REVERSIBLE PSF

When directly applied to the measured surface topography, the stochastic modeling discussed in Sec. 3 is affected by the instrumental PSF (or, more generally, the instrumental OTF). The goal of this section is to find a recipe for determining a TILF that corresponds to the inherent surface topography free of the instrumental perturbation.

Assume that an inherent surface slope trace $X_{SUT} = \left\{ x_{SUT}(n) / n \in \mathbb{Z}^1 \right\}$ ($\mathbb{Z}^1$ is a unit lattice; index 1 denotes one-dimensional integer lattice) is measured at discrete position points $t_n = n \cdot \Delta t$ [$n = 1, \ldots, N$, N is the total number of observations, Δt is the measurement increment, and $L = (N-1)\Delta t$ is the total length of the trace] with a metrology instrument, which is defined to have known symmetrical PSF filter P, centered on the ideal image point, with the weights p_k, $k \in \mathbb{Z}^1$, $p_0 \neq 0$, $p_k = p_{-k}$. In these notations, Eq. (2) can be rewritten as

$$X_{MES} = P * X_{SUT} + E_{MES}, \tag{24}$$

or more explicitly

$$x_{MES}(n) = \sum_k p_k x_{SUT}(n-k) + \varepsilon(n), \tag{25}$$

where $E_{MES} = \left\{ \varepsilon(n) / n \in \mathbb{Z}^1 \right\}$ is the zero-mean random error of the measurement with a standard deviation σ_ε.

Let us also suppose that we found $\tilde{X}_{MES}$ that best fits X_{MES} with an optimal (symmetrical) 'two-sided AR' like TILF model A_{MES} with the weights a_k / $k \in \mathbb{Z}^1$, $a_0 = 0$, $a_k = a_{-k}$ [compare with Eq. (16)]:

$$\tilde{X}_{MES} - X_{MES} = \left(A_{MES} - I \right) * X_{MES} = W \text{ , or } \sum_{l=-p}^{p} a_l \, x_{MES}[n-l] - x_{MES}[n] = w[n], \tag{26}$$

where $W = \left\{ w[n] / n \in \mathbb{Z}^1 \right\}$ is white noise of the TILF model A_{MES}.

Substituting (24) to (26), we get

$$\left(A_{MES} - I \right) * \left(P * X_{SUT} + E_{MES} \right) = W, \tag{27}$$

or, assuming $E_{MES} << W_{SUT}$ (E_{MES} can be made increasingly smaller with averaging of repeatable measurements),

$$P * \left(A_{MES} - I \right) * X_{SUT} = \left(P * A_{MES} - P \right) * X_{SUT} = W. \tag{28}$$

Therefore, the filter

$$C_{SUT} = \left(P * A_{MES} - P\right) \tag{29}$$

is a symmetrical TILF with the weights

$$c_s = \sum_k p_k a_{s-k} - p_s \tag{30}$$

that best fits the inherent surface slope trace X_{SUT}, transforming X_{SUT} to white noise. The symmetry of the filter C_{SUT} (that is $c_s = c_{-s}$) is due to the symmetry of all filters in the right side of Eq. (28).

Normalizing the weights c_s by dividing with $-c_0 = -\sum_k p_k a_k + p_0$, we can rewrite Eq. (28) in terms of an optimal (symmetrical) 'two-sided AR' like TILF A_{SUT} best fit to the inherent trace X_{SUT}:

$$\left(A_{SUT} - I\right) * X_{SUT} = \hat{W}\,, \tag{31}$$

where the weights of the filter A_{SUT} are $\hat{a}_0 = 0$ and $\hat{a}_s = -c_s / c_0$ at $s \neq 0$, and $\hat{W} = \{\hat{w}\,[n] = -w\,[n]/c_0\}$ is white noise of the TILF model A_{SUT}.

Let us now apply a consideration, similar to the one above, to the 'inverse' TILF model B_{MES} that transforms a specially designed (determined in the course of the fitting) white noise sequence (trace) W to a new surface slope trace $\tilde{X}_{MES}$, which best fits the measured one:

$$X_{MES} \approx \tilde{X}_{MES} = B_{MES} * W\,. \tag{32}$$

Substituting (24) to (32) with the condition $E_{MES} << W_{SUT}$, we get

$$P * X_{SUT} \approx B_{MES} * W\,. \tag{33}$$

If the PSF filter P is reversible, we can apply the inverse filter P^{-1} ($P^{-1} * P = I$) to Eq. (33) and get an analytical expression for the TILF model B_{SUT} for X_{SUT}:

$$\tilde{X}_{SUT} \approx P^{-1} * B_{MES} * W = B_{SUT} * W\,. \tag{34}$$

Note that the requirement for reversibility of the PSF filter also arises in the case of straightforward reversing of Eq. (28).

Therefore, in the case of a reversible PSF filter, the TILF model of the slope distribution inherent to the surface under test can be constructed and the new PSF-unperturbed data can be forecast based on the result of optimal TILF modeling of the measured data by using Eq. (34). Correspondingly, the problem of the PSF correction in the statistics domain reduces to a problem of determining the instrumental PSF and its inverse filter.

In Sec. 5 below, we analytically derive the instrumental PSF for the surface slope measurements with an autocollimator based profiler and check if it is reversible.

5. THE OTF AND PSF OF SURFACE SLOPE PROFILERS BASED ON AUTOCOLLIMATOR

In recent publications,[1-6] we applied stochastic modeling to the surface slope variation data obtained with the ALS Developmental Long Trace profiler (DLTP)[41] that is based on a movable pentaprism and an electronic autocollimator (AC) as an angular deflection sensor of the probe light beam. This optical schematic was firstly suggested and realized at the PTB (Germany) by E. Debler and K. Zander in 1978-1980.[42] The current version of the profiler, which is widely used in many metrology laboratories at synchrotron facilities around the world, is the so called Nanometer Optical Measuring Machine (NOM) designed at the HZB/BESSY-II (Germany).[43]

The OTF of the NOM-like profilers, including the ALS DLTP, is determined by an aperture used to limit the size of the AC light sensing the surface under test. In the case of a circular aperture, an analytic expression for the NOM OTF follows up from Fourier transformation

$$OTF_{u,v} = F_{u,v}\left[w(x,y)\right] = \frac{J_1\left(2\pi a\sqrt{u^2+v^2}\right)}{\pi a\sqrt{u^2+v^2}} \tag{35}$$

of a uniform circular weighting function

$$w(x,y) = \begin{Bmatrix} \dfrac{1}{\pi a^2} & x^2+y^2 \le a^2 \\ 0 & x^2+y^2 > a^2 \end{Bmatrix}, \tag{36}$$

where J_1 is the first order Bessel function of the first kind, u and v are the frequency variables, corresponding to the coordinates x and y, respectively, and a is the radius of the aperture.

Note that $w(x,y)$ and $OTF(u,v)$ are inherently 2D functions, corresponding to the 2D shape of the circular aperture. However, the result of a measurement with a profiler is one-dimensional slope trace. In order to reduce the $OTF(u,v)$ to the one corresponding to 1D slope measurement, we can set in (36) $v = 0$:[44]

$$OTF_u = \frac{J_1(2\pi a u)}{\pi a u}. \tag{37}$$

The OFT given with Eq. (37) and shown in Fig. 1 produces low-pass filtering effect with multiple zeros and negative regions where the contrast at those spatial frequencies is reversed.

The result in Eq. (37) has been experimentally verified in the resolution tests with the HZB/BESSY-II NOM. With the use of a specially designed chipped profiled test surface, the 1D optical transfer function OTF_u was directly measured.[37,38] Thus, the high spatial frequency phase shift by π, predicted by (37), was observed.

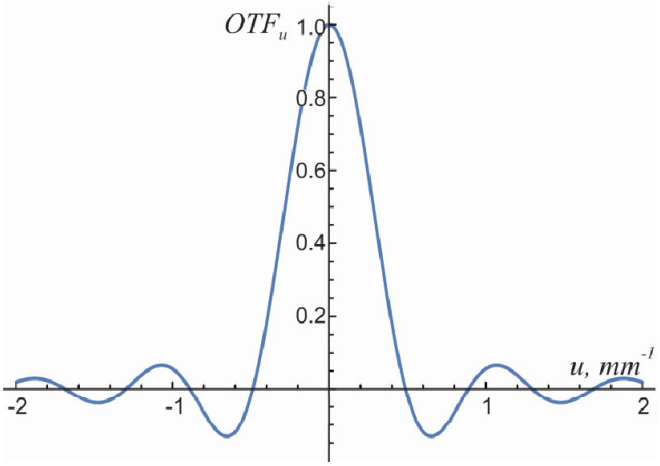

Figure 1. Optical function of an AC-based slope profiler given with Eq. (13) with the radius parameter = 1.25 mm.

At first glance, the shape of the OTF_u in Fig. 1 assumes that most of the high spatial frequency information in a slope trace measured with oversampling (that is with the increment significantly smaller than the instrumental resolution, usually defined as the first zero) has to be lost. However in reality, the information is completely lost only at the zeros of the OTF and a significant portion of the high spatial frequency information can still be reconstructed (see, for example, Ref.[45] and Sec. 6, below).

Applying inverse Fourier transformation to OTF_u, one can derive the 1D PSF of an AC-based slope profiler with circular aperture [compare with Eq. (3)]:

$$PSF_x = \sqrt{\frac{2}{\pi}}\sqrt{a^2 - x^2}\, H\left[4\pi^2\left(a^2 - x^2\right)\right], \tag{38}$$

where $H[z]$ is the Heaviside step function. The function $H[z]$ is a discontinuous function whose value is zero for negative argument and one for positive argument (see, for example, Ref.[46]).

Figure 2 depicts PSF_x given with Eq. (14) for the case of a circular aperture with the diameter of $2a = 2.5$ mm. This size of aperture is commonly used in NOM-like instruments, including the ALS DLTP.[41]

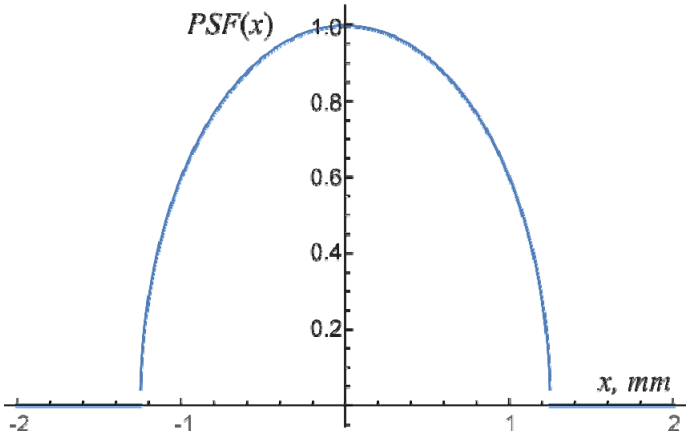

Figure 2. Point spread function of an AC-based slope profiler given with the Heaviside step function with the radius parameter = 1.25 mm.

Note that the PSF in Fig. 2 is different from a rectangular gate function that one would expect in the case of pure 1D instrument with a finite resolution due to a 1D aperture. For such pure 1D instrument, the OTF will be described with a *sinc*-function. Similarly, for a 2D rectangular aperture the instrumental OTF is a product of two *sinc*-functions (see, for example, Refs. [16,17]).

Unfortunately due to the irreversibility of the analytically derived PSF, given with Eq. (38) and shown in Fig. 2, it cannot be directly used to correct the slope data obtained with an AC-based profiler. Nevertheless, a partial correction of the data is still possible.

6. ACCOUNTING OF THE INSTRUMENTAL PSF IN THE CASE OF IRREVERSIBLE PSF FILTER

In this section, we seek to recover (approximate) the slope distribution X_{SUT} inherent to the surface under test assuming that some information on the lost details of X_{SUT} is really present (but 'hidden') in the measured distribution X_{MES} and can be recovered (at least, partially) if we know the details of the perturbation process. For recovering, we construct a mathematical approximation of the instrumental perturbation of the measurement that can be thought of as an approximation $\tilde{P}$ of irreversible PSF filter P, but now possessing the property of reversibility.

Because of the approximate character of the methods, the recovered distribution $\tilde{X}_{SUT}$ is not exactly equal to X_{SUT}. However, if the recovery is successful, the resulted $\tilde{X}_{SUT}$ will contain some additional and significant information about the inherent surface topography X_{SUT} that is not directly seen in the measured trace X_{MES}.

Below in this section, we provide (just as an illustration, unaspiring to any comprehensive covering of this topic) a couple well known solutions to the recovery problem.

6.1 Inverse filtering in Fourier domain

In Fourier (spatial frequency) domain, the convolution relation (24) is

$$F[X_{MES}] = F[P] \cdot F[X_{SUT}] + F[E_{MES}] . \tag{39}$$

If the PSF filter P is known, one can get an estimate $\tilde{F}[X_{SUT}]$ for the Fourier transform of the inherent surface slope trace X_{SUT} by inverse filtering:

$$F[\tilde{X}_{SUT}] \approx \frac{F[X_{MES}]}{F[P]} = F[X_{SUT}] + \frac{F[E_{MES}]}{F[P]} . \tag{40}$$

In order to recover X_{SUT}, one can apply inverse Fourier transform to Eq. (40). Such approach and its multiple variations have been developed for reduction of image blurring (see, for example, Refs.[47-49]). At zero error term, $\sigma_\varepsilon = 0$, the inverse filter in Eq. (40) gives an exact solution.

However at nonzero error, the result of recovering tends to be very sensitive to the measurement error. At the spatial frequencies where $F[P]$ is significantly small, the function $1/F[P]$ can lead to strong enhancement of the error term and, therefore, corruption of the reconstruction. Moreover, in general the optical transfer function $F[P]$ has, besides multiple zeros, negative regions (see, for example, Fig. 1) that result in severe perturbation of the measured trace due to the reverse of the contrast at these spatial frequencies (see discussion in Sec. 5).

Different methods have been developed to reduce the error sensitivity in reverse filtering. The simplest solution is to limit the inverse filter $1/F[P]$ to some threshold ξ and ignore the regions where the error term is dominating:

$$H(u) = \begin{cases} \dfrac{1}{F[P]}, & \text{if} \quad |F[P]| > \xi \\ \xi \dfrac{|F[P]|}{F[P]}, & \text{otherwise.} \end{cases} \tag{41}$$

This threshold inverse filter $H(u)$ can be optimized by careful selection of the threshold. Such an optimization is provided with Wiener optimal filter,[48,49] briefly discussed in Sec. 6.2, below.

6.2 Wiener optimal filter

In application to the reconstruction of surface slope topography, the Wiener optimal filter provides a reconstruction $\tilde{X}_{SUT}$ that minimizes the least mean square error to the inherent surface topography X_{SUT}. Due to the unitary property of the Fourier transform, there is the same information in the real and Fourier domain. Therefore, if $\tilde{X}_{SUT} \approx X_{SUT}$, the corresponding Fourier transforms are also close, $F[\tilde{X}_{SUT}] \approx F[X_{SUT}]$, and the least squares method can be applied in the Fourier domain. The minimization variable is the inverse filter $H(u)$ [compare with Eq. (41)]:

$$F[\tilde{X}_{SUT}] = F[X_{MES}] H(u) = F[X_{SUT}] F[P] H(u) + F[E_{MES}] H(u) , \tag{42}$$

so that

$$\frac{\partial}{\partial H} \left\langle \left| F[\tilde{X}_{SUT}] - F[X_{SUT}] \right|^2 \right\rangle = 0 . \tag{43}$$

Substitution of (42) to (43) gives

$$\frac{\partial}{\partial H} \left\langle \left| F[X_{SUT}] - F[X_{SUT}] F[P] H(u) - F[E_{MES}] H(u) \right|^2 \right\rangle = 0 . \tag{44}$$

Using straightforward algebraic transformation and assuming independent and zero-mean error distribution, one can derive the Wiener optimal filter expressed through the corresponding PSDs in the following form (see, for example, Ref.[48]):

$$H(u)=\frac{F^{*}[P]}{\left|F[P]\right|^{2}+\dfrac{\left|F[E_{MES}]\right|^{2}}{\left|F[X_{SUT}]\right|^{2}}}=\frac{F^{*}[P]}{PSD[P]+\dfrac{PSD[E_{MES}]}{PSD[X_{SUT}]}}, \tag{45}$$

where $F^{*}[P]$ is the complex conjugate of $F[P]$.

Practical application of the Wiener optimal filter (45) needs to overcome the generally unknown PSD of the ideal trace $PSD[X_{SUT}]$. There are a number of possible approximations.[49] The one that allows solving the reconstruction problem in the case of the DLTP measurements with the PSF derived in Sec. 5 is discussed in the next section.

7. CORRECTION OF THE TILF MODEL DETERMINED FOR THE MEASURED SURFACE SLOPE DATA TO ACCOUNT THE PERTURBATION DUE TO THE INSTRUMENTAL PSF

The idea behind the simulations, described in this section, is to apply the reconstruction procedure in Sec. 6.2 to an artificial X_{MES}, obtained by convolution of X_{SUT}, generated with a known TILF, and a PSF in Sec. 5, corresponding to the measurements with the ALS DLTP,[41] and addition of a white noise like 'measurement' error [compare with Eq. (24)]. This approach allows us to evaluate the efficiency of the procedure by comparing the result of the reconstruction $\tilde{X}_{SUT}$ with the 'inherent' (generated) X_{SUT}.

In order to generate X_{SUT} trace of the total length of 180 mm and the increment of 0.2 mm, we use an optimal symmetrical TILF (two sided symmetrical ARMA model) determined in Ref.[5,6] by modeling surface slope distribution, measured with the SLAC Linac Coherent Light Source (LCLS) beam split and delay mirror[50] by using the DLTP. Figure 3 depicts the generated 'inherent' surface slope trace, X_{SUT}.

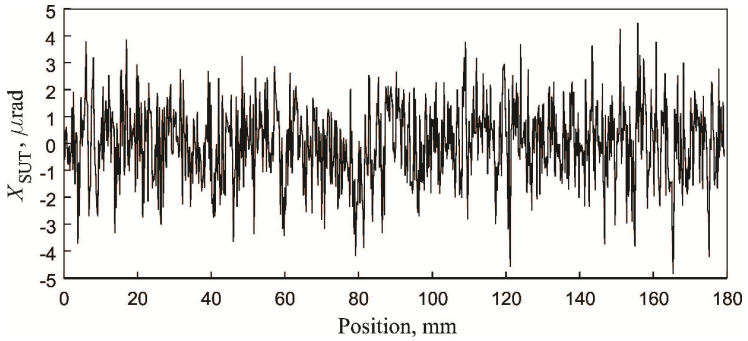

Figure 3. Slope trace X_{SUT} generated with the TILF model[41] of the LCLS beam split and delay mirror[50] and used as an inherent surface stochastic topography in the simulations discussed in the text.

The measured trace X_{MES} is obtained as a convolution of X_{SUT} and the PSF given by Eq. (14) with the diameter of the circular aperture of $2a = 2.5$ mm. The variation of the white noise added to the result of the convolution is 1/6 of that of the inherent trace X_{SUT}.

The simulated 'measured' trace, X_{MES} is shown in Fig. 4. The perturbative effect of the instrumental PSF to the surface slope measurement can be seen as strong filtering (smoothing) leading to a significant, by a factor of approximately 2.5, decrease of the surface slope variation from 1.49 μrad (rms) for the 'inherent' topography to 0.60 μrad (rms) for the 'measured' one.

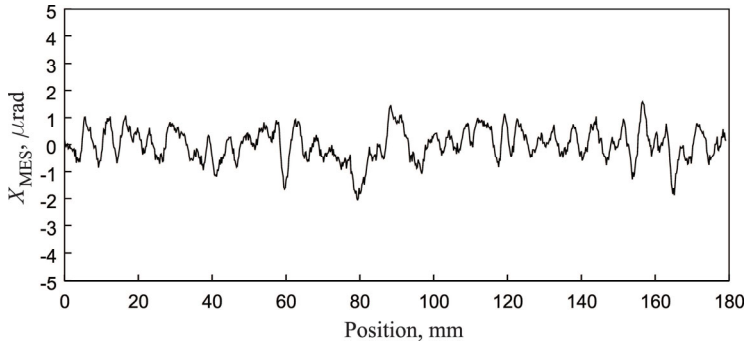

Figure 4. Slope trace X_{MES} obtained as a convolution of X_{SUT} in Fig. 3 and the PSF given by Eq. (14) with the diameter of the circular aperture of $2a = 2.5$ mm. In the simulations, the trace is used as the measured surface stochastic topography.

For reconstruction of $\tilde{X}_{SUT}$ from X_{MES}, we apply the Wiener optimal filter (45) constructed with the known PSF filter, the PSD of the 'inherent' trace $PSD[X_{SUT}]$, and with the constant PSD of the measurement noise used to simulate X_{MES}.

The result of the reconstruction is shown in Fig. 6. The rms variation of the reconstructed trace in Fig.5 is 1.18 μrad (rms) that is only about 20% less than that of the 'inherent' trace.

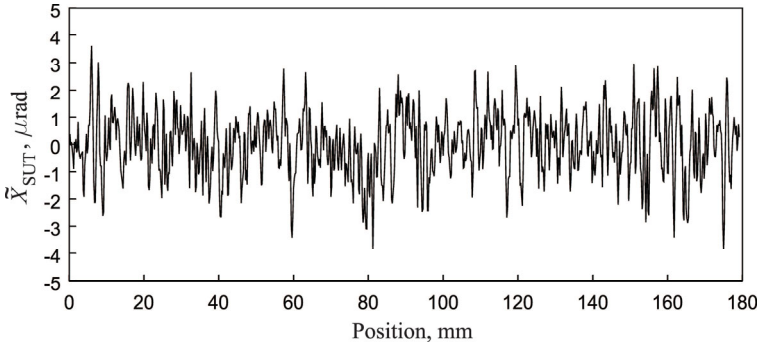

Figure 5. Slope trace $\tilde{X}_{SUT}$ reconstructed from X_{MES} by applying the Wiener optimal filter (45) constructed as described in the text.

For better visual comparison of the reconstructed trace $\tilde{X}_{SUT}$ with X_{SUT} and X_{MES}, the all three slope traces are shown in Fig. 6 over a reduced surface area.

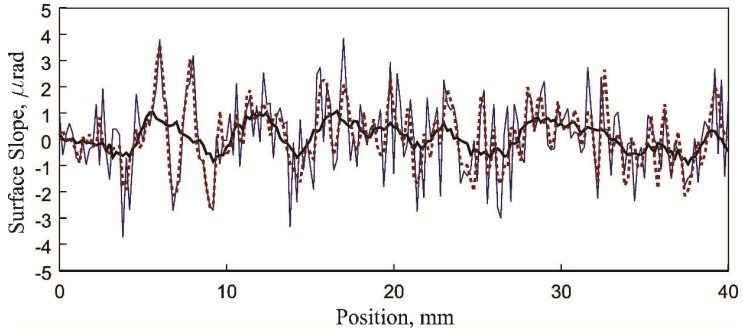

Figure 6. The 'inherent' slope trace X_{SUT} (blue thin solid line) and the slope trace $\tilde{X}_{SUT}$ (red dashed line) reconstructed by applying the Wiener optimal filter to X_{MES} (black bold solid line).

The reconstructed trace, shown in Fig. 6 with red dashed line, reproduces a significant portion of higher spatial variation of the 'inherent' trace (blue thin solid line) that is filtered out in the 'measured' trace (black bold solid line). This is an indication of the corresponding increase of effective resolution of the measurement that is possible due to the reconstruction.

Practically, the reconstructed trace can be directly modeled with the TILF method providing more reliable approximation to the TILF model of the inherent surface topography. Alternatively, the TILF determined in modeling of the measured trace can be corrected using the approximate inverse PSF obtained from inverse Fourier transformation of the Wiener optimal filter used for the reconstruction (see Sec. 5).

8. DISCUSSION AND CONCLUSIONS

In this work, we have first formulated and briefly outlined a new direction of research on development of methods for statistical modeling of surface topography of state-of-the-art x-ray mirrors.[1-6] This is the creation of a single-model (hybrid) statistical description of SUT topography by combining statistical models determined from metrology data obtained with different instruments designed for measurements over significantly different spatial wavelength ranges. This can be thought of as a problem of stitching the data in the statistical domain.

A determined hybrid statistical model will provide a uniform statistical description of the mirror surface topography over the entire spatial frequency range, important for the particular beamline application of the mirror. Moreover, the hybrid model will provide a tool to forecast the required uniform data based on surface topography data, obtained using various instruments, for optics made by the same vendor and technology. The forecast data is vital for reliable specification for optical fabrication, evaluated from numerical simulation to be exactly adequate for the required system performance, avoiding both over- and under-specification.

We have formulated and suggested how to solve a fundamental problem of the statistical modeling that is a reliable accounting of the imperfections in the instruments described by the instrumental point spread function.

For the case of a reversible PSF, we have derived an analytical transformation of the TILF model determined for the measured data to the one valid for the inherent surface topography. Unfortunately, such a solution is not applicable to surface slope measurements performed with an auto-collimator based deflectometer, where, as we have analytically shown, the PSF is irreversible.

For the case of an irreversible PSF, we suggested an approximate solution that utilizes mathematical methods developed for recovering of blurred images. We have provided an introduction to the mathematical foundation of the recovery methods and outlined a derivation of the Wiener optimal filter that seems to be one of the most suitable solutions in our case. The high efficiency of the Wiener optimal filter approach to the slope data restoration has been verified on the surface slope data forecasted based on the TILF model determined from a real x-ray mirror in Refs.[5,6]

In conclusion, we would like to specially emphasize that the solution of the PSF irreversibility problem, described in this note, provides a method for partial reconstruction, from oversampled data, of surface variations above the spatial frequency range determined by the resolution.

ACKNOWLEDGEMENT

The authors are very grateful to Daniel J. Merthe, Nikolay A. Artemiev, and Daniele Cocco for help with high accuracy surface slope measurements of the LCLS beam split and delay mirror, and to Gary Centers and Wayne McKinney for very useful discussions. This work was supported in part by NASA Small Business Innovation Research SBIR grant to Second Star Algonumerics, project No. 15-1 S2.04-9193. The Advanced Light Source is supported by the Director, Office of Science, Office of Basic Energy Sciences, Material Science Division, of the U.S. Department of Energy under Contract No. DE-AC02-05CH11231 at Lawrence Berkeley National Laboratory.

expressed herein do not necessarily state or reflect those of the United States Government or any agency thereof or The Regents of the University of California.

REFERENCES

[1] Yashchuk, Y. V. and Yashchuk, V. V., "Reliable before-fabrication forecasting of expected surface slope distributions for x-ray optics," Proc. SPIE 8141, 81410N-1-15 (2011); doi: 10.1117/12.893775.
[2] Yashchuk, Y. V. and Yashchuk, V. V., "Reliable before-fabrication forecasting of expected surface slope distributions for x-ray optics," Opt. Eng. 51(4), 046501 (2012); http://dx.doi.org/10.1117/1.OE.51.4.046501.
[3] Yashchuk, V. V., Tyurin, Y. N., and Tyurina, A. Y., "Application of time-invariant linear filter approximation to parameterization of one- and two-dimensional surface metrology with high quality x-ray optics," Proc. SPIE 8848, 88480H-1-13 (2013).
[4] Yashchuk, V. V., Tyurin, Y. N., and Tyurina, A. Y., "Application of the time-invariant linear filter approximation to parametrization of surface metrology with high-quality x-ray optics," Opt. Eng. 53(8), 084102 (2014).
[5] Yashchuk, V. V. , Tyurin, Yu. N., and Tyurina, A. Yu., "Modeling of surface metrology of state-of-the-art x-ray mirrors as a result of stochastic polishing process," Proc. SPIE 9809, 98090M/1-16 (2015); doi:10.1117/12.2218750 1-16.
[6] Yashchuk, V. V. , Tyurin, Yu. N., and Tyurina, A. Yu., "Modeling of surface metrology of state-of-the-art x-ray mirrors as a result of stochastic polishing process," Opt. Eng. 55(7), 074106 (2016); doi: 10.1117/1.OE.55.7.074106.
[7] Yashchuk, V. V., Samoylova, L., and Kozhevnikov, I. V., "Specification of x-ray mirrors in terms of system performance: new twist to an old plot," Opt. Eng., 54(2), 025108 (2015).
[8] Yashchuk, V. V., Samoylova, L., and Kozhevnikov, I. V., "Specification of x-ray mirrors in terms of system performance: A new twist to an old plot," Proc. SPIE 9209, 92090F/1-19 (2014).
[9] Mimura, H., Yumoto, H., Matsuyama, S., Yamamura, K., Sano, Y., Ueno, K., Endo, K., Mori, Y., Yabashi, M., Tamasaku, K., Nishino, Y., Ishikawa, T. and Yamauchi, K., "Relative angle determinable stitching interferometry for hard x-ray reflective optics," Rev. Sci. Instrum. 76, 045102 (2005).
[10] Yumoto, H., Mimura, H., Handa, S., Kimura, T., Matsuyama, S., Sano, Y., Ohashi, H., Yamauchi, K. and Ishikawa, T., "Stitching-angle measurable microscopic-interferometer: Surface-figure metrology tool for hard X-ray nanofocusing mirrors with large curvature," Nucl. Instr. and Meth. A 616(2-3), 203-206 (2010).
[11] Boreman, G. D. [Modulation Transfer Function in Optical and Electro-optical Systems], SPIE Press, Bellingham, Washington (2001).
[12] Yashchuk, V. V., Irick, S. C., Gullikson, E. M., Howells, M. R., MacDowell, A. A., McKinney, W. R., Salmassi, F., and Warwick, T., "Cross-check of different techniques for two-dimensional power spectral density measurements of X-ray optics," Proc. SPIE 5921, 59210G-1-12 (San Diego, California, USA, 2-3 August 2005).
[13] Yashchuk, V. V., Gullikson, E. M., Howells, M. R., Irick, S. C., MacDowell, A. A., McKinney, W. R., Salmassi, F., Warwick, T., Metz, J. P., and Tonnessen, T. W., "Surface Roughness of Stainless Steel Mirrors for Focusing Soft X-rays," Appl. Opt. 45(20) 4833-4842 (2006).
[14] Yashchuk, V. V., Franck, A. D., Irick, S. C., Howells, M. R., MacDowell, A. A., and McKinney, W. R., "Two dimensional power spectral density measurements of X-ray optics with the Micromap interferometric microscope," Proc. SPIE 5858, 58580A-1-12 (2005).
[15] Takacs, P. Z., Barber, S., Church, E. L., Kaznatcheev, K., McKinney, W. R., and Yashchuk, V. V., "2D Spatial Frequency Considerations in Comparing 1D Power Spectral Density Measurements," in Optical Fabrication and Testing, OSA Technical Digest (CD) (Optical Society of America, 2010), paper OWE5.
[16] Kay, S. M., [Modern Spectral Estimation: Theory and Application], Prentice Hall, Englewood Cliffs (1988).
[17] Jenkins, G. M. and Watts, D. G., [Spectral Analysis and its Applications], Fifth Printing: Emerson-Adams Press, Boca Raton (2007).
[18] Yashchuk, V. V., Artemiev, N. A., Lacey, I., McKinney, W. R., and Padmore, H. A., "A new x-ray optics laboratory (XROL) at the ALS: Mission, arrangement, metrology capabilities, performance, and future plans," Proc. SPIE 9206, 92060I -1-19 (2014) [doi:10.1117/12.2062042].
[19] Yashchuk, V. V., Artemiev, N. A., Lacey, I., McKinney, W. R., and Padmore, H. A., "Advanced environmental control as a key component in the development of ultra-high accuracy ex situ metrology for x-ray optics," Opt. Eng. 54(10), 104104/1-14 (2015) [doi: 10.1117/1.OE.54.10.104104].

[20] Yashchuk, V. V., McKinney, W. R., and Takacs, P. Z., "Test Surfaces Useful For Calibration Of Surface Profilometers," U.S. patent application 20100037674 (18 February 2010); U.S. patent 8,616,044 (31 December 2013).
[21] Yashchuk, V. V., McKinney, W. R., and Takacs, P. Z., "Binary Pseudorandom Grating Standard for Calibration of Surface Profilometers," Proc. SPIE 6704, 670408 (2007); Opt. Eng. 47(7), 073602 (2008).
[22] Barber, S. K., Soldate, P., Anderson, E. D., Cambie, R., McKinney, W. R., Takacs, P. Z., Voronov, D. L., and Yashchuk, V. V., "Development of Pseudo-random Binary Gratings and Arrays for Calibration of Surface Profile Metrology Tools," J. Vac. Sci. and Tech. B 27(6), 3213 (2009).
[23] Barber, S. K., Anderson, E. D., Cambie, R., McKinney, W. R., Takacs, P. Z., Stover, J. C., Voronov, D. L., and Yashchuk, V. V., "Binary Pseudo-Random Gratings and Arrays for Calibration of Modulation Transfer Function of Surface Profilometers," Nucl. Instr. and Meth. A 616, 172 (2010).
[24] Barber, S. K., Soldate, P., Anderson, E. D., Cambie, R., Marchesini, S., McKinney, W. R., Takacs, P. Z., Voronov, D. L., and Yashchuk, V. V., "Binary Pseudo-random Gratings and Arrays for Calibration of the Modulation Transfer Function of Surface Profilometers: Recent Developments," Proc. SPIE 7448, 744802-1-12 (2009).
[25] Barber, S. K., Anderson, E. D., Cambie, R., Marchesini, S., McKinney, W. R., Takacs, P. Z., Voronov, D. L., and Yashchuk, V. V., "Stability of modulation transfer function calibration of surface profilometers using binary pseudo-random gratings and arrays with non-ideal groove shapes," Opt. Eng. 49(5), 053606 (2010).
[26] Yashchuk, V. V., Anderson, E. H., Barber, S. K., Bouet, N., Cambie, R., Conley, R., McKinney, W. R., Takacs, P. Z., and Voronov, D. L., "Calibration of the modulation transfer function of surface profilometers with binary pseudo-random test standards: expanding the application range to Fizeau interferometers and electron microscopes," Opt. Eng. 50(9), 093604 (2011).
[27] Yashchuk, V. V., Conley, R., Anderson, E. H., Barber, S. K., Bouet, N., McKinney, W. R., Takacs, P. Z., and Voronov, D. L., "Characterization of electron microscopes with binary pseudo-random multilayer test samples," Nucl. Instr. and Meth. A 649(1), 150 (2011).
[28] Babin, S., Calafiore, G., Peroz, C., Conley, R., Bouet, N., Cabrini, S., Chan, E., Lacey, I., McKinney, W. R., Yashchuk, V. V., and Vladar, A., "1.5 nm fabrication of test patterns for characterization of metrological systems," J. Vac. Sci. and Technol B 33(6), 06FL01/1-5 (2015) [doi: 10.1116/1.4935253].
[29] Yashchuk, V. V., Fischer, P. J., Chan, E. R., Conley, R., McKinney, W. R., Artemiev, N. A., Bouet, N., Cabrini, S., Calafiore, G., Lacey, I., Peroz, C., and Babin, S., "Binary pseudo-random patterned structures for modulation transfer function calibration and resolution characterization of a full-field transmission soft x-ray microscope," Rev. Sci. Instrum. 86(12), 123702/1-12 (2015) [doi: 10.1063/1.4936752].
[30] Bardell, P. H., McAnney, W. H., Savir, J., [Built-in test for VLSI pseudorandom techniques], John Wiley and Sons, Inc., New York (1987).
[31] Busboom, A., Elders-Boll, H., and Schotten, H. D., "Uniformly Redundant Arrays," Experimental Astronomy: Astrophysical Instrumentation and Methods 8, 97 (1998).
[32] Sclar, B., [Digital Communications: Fundamentals and Applications], 2nd Ed., Prentice Hall (2001).
[33] Etzon, T., "Construction for perfect maps and pseudo-random arrays," IEEE Trans. on Information Theory 34(5), 1308 (1988).
[34] Koleske, D. D., and Sibener, S. J., "Generation of pseudo-random sequence for use in cross-correlation modulation," Rev. Sci. Instrum. 63(8), 3852 (1992).
[35] Mitra, A., "On pseudo-random and orthogonal binary spreading sequences," International Journal of Information and Communication Engineering 4(6), 447 (2008).
[36] Chu, W.T., "Impulse-Response and Reverberation-Decay Measurements Made by Using a Periodic Pseudorandom Sequence," Appl. Acoustics 29, 193 (1990).
[37] Siewert, F., Zeschke, T., Arnold, T., Paetzold, H., and Yashchuk, V., "Linear chirped slope profile for spatial calibration in slope measuring deflectometry," Rev. Sci. Instrum. 87(5), 051907 (2016); doi: 10.1063/1.4950737.
[38] Siewert, F., Buchheim, J., Zeschke, T., Arnold, T., Paetzeld, H., and Yashchuk, V. V., "Chirped profile for spatial calibration in slope measuring deflectometry," Abstract to The International Workshop on Metrology for X-ray Optics, Mirror Design, and Fabrication, Satellite Workshop at the 12th International Conference on Synchrotron Radiation Instrumentation, SRI 2018 (Berkeley, USA, July 13-16, 2015).
[39] EViews 8 User's Guide, Volumes I and II, Quantitative Micro Software; www.eviews.com.
[40] Brockwell, P. J. and Davis, R. A., [Time Series: Theory and Methods], Second Ed., Springer, New York (2006).
[41] Yashchuk, V. V., Barber, S., Domning, E. E., Kirschman, J. L., Morrison, G. Y., Smith, B. V., Siewert, F., Zeschke, T., Geckeler, R., and Just, A., "Sub-microradian surface slope metrology with the ALS Developmental Long Trace Profiler," Nucl. Instrum. and Methods A 616(2-3), 212-223 (2010) [doi:10.1016/j.nima.2009.10.175].

[42] Debler, E., and Zander, K., “Measurement of evenness on optical plane surfaces with autocollimator and pentagon prism, PTB-Mitteilungen 90(5), 339-349 (1980).
[43] Siewert, F., Lammert, H., and Zeschke, T., “The nanometer optical component measuring machine,” in: [Modern Developments in X-Ray and Neutron Optics], Erko, A., Idir, M., Krist, T., and Michette, A. G., Eds., Springer, New York (2008).
[44] Merthe, D. J., and Yashchuk, V. V., “Measurements of Chirped Functions on Surfaces with Finite Areal Resolution,” LSBL Note LSBL-1151 (Berkeley, November 19, 2012).
[45] Easton, R. L., [Fourier methods in imaging], 1st ed., Wiley (2010); Ch. 19: “Applications of linear filters.”
[46] Davies, B., [Integral Transforms and their Applications], 3rd ed., Springer, (2002); p. 28: “Heaviside step function.”
[47] Lim, J. S., [Two-dimensional signal and image processing], P.T.R. Prentice-Hall, Englewood Cliffs (2010); Ch. 9: “Image restoration.”
[48] Wiener, N., [Extrapolation, Interpolation, and Smoothing of Stationary Time Series], Martino Publishing, Mansfield Centre, CT (2013).
[49] Grigoryan, A. M., Dougherty, E. R., Agaian, S. S., “Optimal Wiener and homomorphic filtration: Review,” Signal Processing 121(C), 111-138 (2016); doi: 10.1016/j.sigpro.2015.11.006.
[50] B. Murphy, X-Ray Split and Delay Mirrors Specifications, Drawings PF-391-946-11 and SA-391-946-13, LCLS, Menlo Park (2011).